Composite Structures 210 (2019) 430–445

Contents lists available at ScienceDirect

Composite Structures

journal homepage: www.elsevier.com/locate/compstruct

Structure-property relationship for a prepreg platelet molded composite with engineered meso-morphology

Sergii G. Kravchenko[a,*], Drew E. Sommer[a], Benjamin R. Denos[a], William B. Avery[b], R. Byron Pipes[a]

[a] Composites Manufacturing & Simulation Center, Purdue University, 1105 Challenger Av., Suite 100, West Lafayette, IN 47906, United States
[b] Boeing Commercial Airplanes, P.O. Box 3707, Seattle, WA 98124, United States

ARTICLE INFO

Keywords:
Discontinuous reinforcement
Mechanical properties
Damage mechanics
Prepreg platelet

ABSTRACT

The objective of this work was to develop a finite-element based computational model to investigate the complex three-dimensional load transfer from the known meso-structure of a prepreg platelet molded composite (PPMC) system with a layered planar morphology and deterministic orientation state, where platelets are aligned and staggered in each layer. Three-dimensional stress transfer was studied for the prediction of failure under tensile loading. A finite-element model was used for the analysis of the composite structure-property relationship. Variability of meso-structure geometry was shown to control the distributed tensile properties of a PPMC laminate. Platelet length-to-thickness and length-to-width ratios were found to control the composite effective strength. Experimental analysis was used to complement the results of theoretical studies. A PPMC meso-structure with deterministic orientation state of engineered morphology was found to provide enhanced effective tensile properties with reduced variability as compared to stochastic prepreg platelet meso-structure. The mechanisms leading to enhanced structural performance were (i) the improved hierarchical structure of the platelet system and (ii) the ability to define the fiber orientation state of the composite system.

1. Introduction

Composite systems molded from the prepreg platelets have been shown to demonstrate improved performance over the systems manufactured from traditional sheet molding compounds [1,2]. Prepreg platelets are obtained by transforming continuous fiber (CF) precursor prepreg tape, of given thickness, into discontinuous pieces of assigned length and width [1]. Compression or transfer molding of such platelets results in composite with complex meso-scale structure, which is semi-laminated and platelet level heterogeneous, to provide for sufficient formability characteristics [2,3] and enhanced mechanical properties [4]. The meso-scale structure [5] of a prepreg platelet molded composite (PPMC) is defined by the system morphology and platelet geometrical parameters, Fig. 1(a). The number and geometrical accommodation (arrangement/overlap and orientation) of platelets determine the meso-scale morphology of a PPMC. Clearly, orientation state, describing how the platelets are oriented with respect to one another spatially and aligned with the loading direction, is one of the important morphology descriptors in a PPMC meso-structure. In continuous fiber laminates, the orientation state is achieved by a specified stacking sequence of prepreg ply orientations. The orientation state in a PPMC can be stochastic (uncontrolled) or deterministic (controlled, or engineered) depending on the manufacturing approach, as schematically shown in Fig. 1(b).

Multi-directionality of platelet orientations is a prominent feature and one of the primary assets of a PPMC because the composite functionality can be designed through the fiber orientation control [6]. Platelet orientations in multiple directions are desired for structural applications of composites since differently oriented fibers allow the composite to react more specifically to the force transmission in the target component. By changing the orientation state in a controlled way, the composite properties can be fitted to the desired external loads.

A stochastic form of a PPMC is achieved when the orientation and arrangement disorder result from the uncontrolled positioning of platelets into the mold followed by molding flow. A stochastic PPMC is often referred to as having a “random” orientation distribution, but in this context “random” should not be always considered equivalent to “uniformly distributed probability.” Inability to control material structure formation creates an obstacle for composite properties

* Corresponding author.
E-mail address: skravche@purdue.edu (S.G. Kravchenko).

https://doi.org/10.1016/j.compstruct.2018.11.058
Received 1 August 2018; Received in revised form 24 October 2018; Accepted 21 November 2018
Available online 22 November 2018

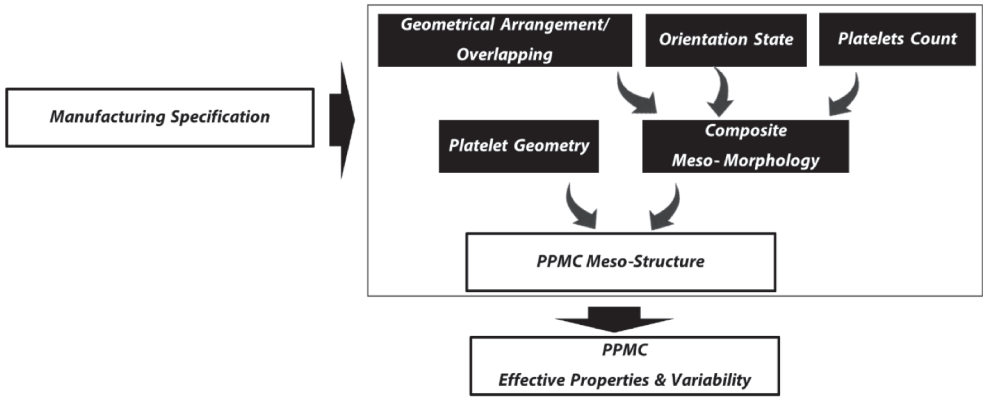

(a)

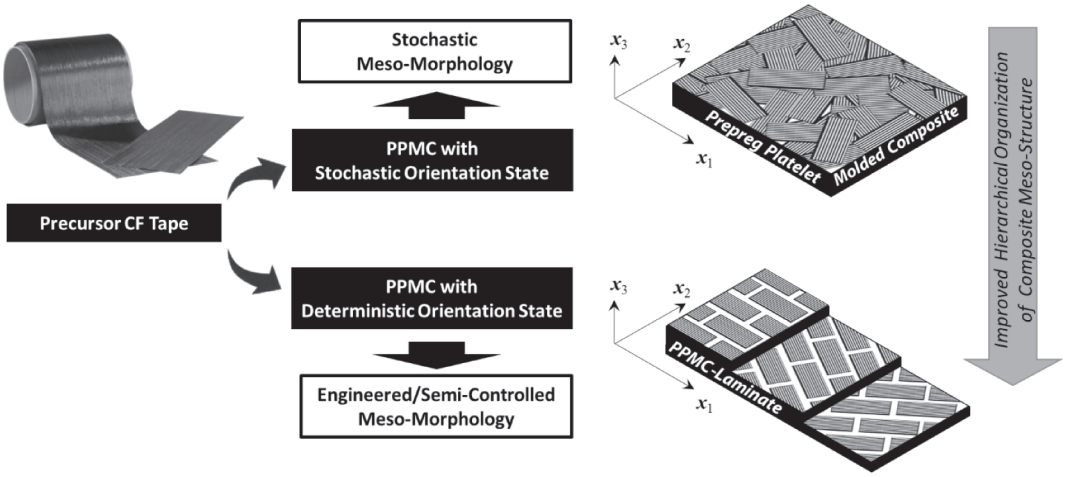

(b)

Fig. 1. (a) Definition of the meso-structure of a prepreg platelet molded composite (PPMC); (b) Morphological forms of a PPMC.

control. Several research groups have previously reported a high level of variability in effective tensile properties of such composite systems attributed to the stochastic nature of their uncontrolled morphology [4,7–12].

Alternatively, a semi-controlled morphology with a deterministic orientation state can be engineered for a PPMC while maintaining processability and scalability of manufacturing. A regular pattern of cross-fiber cuts is introduced into the CF prepreg ply to produce a sheet of aligned and staggered platelets, as reported by Taketa et al. [13,14], who coined a term “unidirectionally arrayed chopped strands” (UACS) for such a sheet. Arranging the UACS sheets at different angles produces a multi-directional PPMC laminate with a controlled orientation state. The formation of hierarchical arrangements in a PPMC morphology provides the structural basis for enhancing effective properties of the composite system [15]. Although in practice the overlap distribution between platelets from adjacent plies in a PPMC laminate is obtained in a non-controlled way and is essentially non-deterministic, a deterministic orientation state provides for a reduced variability of PPMC laminate meso-structure as compared to a stochastic PPMC and consequently the reduced variability of mechanical properties is expected.

The mechanical behavior of a PPMC is determined by the properties of the individual platelets and the meso-scale interactions between platelets, both of which control the load transmission through the composite system. Therefore, the assembled structure of the composite governs the stress transfer and strongly influences failure mechanisms and strength. The first challenge in designing a load-carrying meso-structure is to establish a relationship between the structure and the resulting mechanical properties [16–21].

The objective of this work is to develop a finite-element based computational model to investigate the complex three-dimensional stress transfer from the known meso-structure of a PPMC system with a layered planar morphology and deterministic orientation state. This allows one to tailor the effective properties in response to the changes in composite structure and thereby examine the structure-property relationship in order to understand potential property limits of the composite. Specifically, the influence of the platelet geometrical parameters is studied for the effective quasi-static tensile properties, which are among those of primary importance when a composite system is considered for a design application [22]. The macroscopic failure of the composite structure emerges from the evolution and interaction of local sub-scale failure events in composite elements. A comprehensive methodology for the analysis of composite structure should account for all damage modes and their interactions. The meso-scale failures that develop within a prepreg platelet based system include platelet transverse damage (platelet splitting along the fibers), debonding between adjacent platelets (delamination) and failure transverse to the platelet fiber direction (fiber fracture). A composite system made up of a large number of platelets is a complex system with substantial internal

redundancy. This means that the onset of failure in just a few individual platelets generally does not immediately lead to the complete system failure. The redundant system will gradually deteriorate before it accumulates enough sub-critical damage for the overall ultimate failure. This is why a progressive failure analysis (PFA) approach is herein used to study the failure of these systems. A continuum damage mechanics-based constitutive model is utilized for platelet orthotropic damage modes. Surface-based cohesive behavior determined by the traction-separation constitutive model is defined for contacting layers of platelets to model delamination. The finite element analysis is performed in ABAQUS/Standard (Implicit) [23].

From computational analysis, both platelet length-to-thickness (L_p/t_p) and length-to-width (L_p/w_p) ratios are found to influence the strength of a PPMC laminate. The effect of platelet width on effective tensile strength in a PPMC with engineered morphology is experimentally investigated to complement the theoretical analysis. The variability of meso-structure geometry in a PPMC laminate (i.e. the distribution of overlaps between platelets) for a defined orientation state is shown to translate into the variability of composite effective tensile properties. The thermo-elastic analysis of the meso-scale thermal-residual stresses followed by the progressive failure analysis showed that the ultimate tensile strength of a PPMC-laminate is not substantially affected by the thermal-residual stresses.

2. Experimental work

In the following sections, the composite fabrication and the experimental test procedure are outlined. The platelet parent material was the AS4/PEKK unidirectional continuous fiber prepreg tape (Cytec/Solvay). The effect of meso-structure with stochastic and deterministic orientation state on the quasi-static effective tensile modulus and strength of a PPMC is considered. The tensile properties of a stochastic PPMC are used as a baseline to illustrate the performance improvement through morphology control. The discussion of experimental results is divided into two parts: (i) the dependence of PPMC properties variability on material structure and (ii) platelet width effect for an engineered morphology.

2.1. Manufacturing of coupons with stochastic and deterministic orientation states

PPMC coupons with multi-directional layers of aligned and staggered prepreg platelets were manufactured for testing in displacement control uniaxial tension. The aligned platelets were oriented into planar staggered arrays during the preforming stage. This was achieved by introducing regular discontinuous cuts across the continuous fibers of AS4/PEKK unidirectional prepreg tape. A drag knife on a Gerber cutting machine mechanically introduced the cross fiber cuts with intervals defining the platelet length, L_p, while the cut length sets the platelet width, w_p, as seen in Fig. 2(a). The cut intervals were 0.5 in (12.7 mm)-long and two cut widths were considered, 0.5 in (12.7 mm) and 0.125 in (3.175 mm), resulting in L_p/w_p ratios of 1 and 4, respectively. Taketa and co-workers [13] termed the resulting special sheet with patterned slits as “unidirectionally arrayed chopped strands” (UACS). Photographs of the prepreg samples with cross fiber cuts distribution pattern are shown in Fig. 2(a). After the cuts were introduced, the sheets were stacked into the lamination sequence of $[0^\circ/\pm 45^\circ/90^\circ/\mp 45^\circ/0^\circ]$ ($[0^\circ/\pm 45^\circ/90^\circ_{1/2}]_s$ for short) resulting in PPMC with engineered morphology having a controlled orientation state (a UACS-laminate if using Taketa’s terminology). Slit prepreg is an induced discontinuity type of aligned discontinuous fiber reinforcement according to classification by Such et al. [24]. The PPMC-laminates were assembled into the 10 × 10 in mold cavity, put into the oven to reach 380 °C and then pressed with a pressure of 1000 psi (6.89 MPa, or 68.9 bar). After pressing, the laminate was tabbed and cut into 10 in long test coupons having the gage length, L, of 6 in (152.4 mm) and width, w, of 1 in (25.4 mm), schematically shown in Fig. 3(a). The average thickness of five $[0^\circ/\pm 45^\circ/90^\circ_{1/2}]_s$ coupons, t, for both $L_p/w_p = 1$ and 4, was 0.91 mm with coefficient of variance (cov) of 6.7% and 5.1%, respectively.

The additional five tensile coupons were manufactured from a plaque molded of random disordered 0.5 × 0.5 in (12.7 × 12.7 mm) prepreg platelets. The charge of loose platelets was poured into the mold to achieve full coverage providing no control over platelets orientation or arrangement during the deposition stage. The average thickness, t, of coupons with stochastic morphology was 0.79 mm (cov. 7.1%). Coupons had a final gage length, L, of 152.4 mm (6 in) and width, w, of 25.4 mm (1 in).

2.2. DIC-complemented quasi-static tension test

The elastic and strength properties were assessed by quasi-static tension test. The coupons were coated with white spray paint and a random black speckle pattern was applied for digital image correlation (DIC), as schematically shown in Fig. 3(a). Tensile tests were performed using a 22 kip-MTS material-testing system in displacement control with crosshead rate of 2 mm/min. Coupons were loaded in the test frame while being monitored by the VIC-SNAP DIC system provided by Correlated Solution Inc. DIC was used to measure coupon surface displacements under stress and further use the displacements to calculate full field Green-Lagrangian strain distribution $\epsilon_{11}(x_1, x_2)$ during loading history. The DIC analysis was performed with VIC-3D software using a subset size of 31 pixels and a strain filter of 7 pixels with 0.6 pixel/mm.

2.3. Experimental analysis of effective stiffness and strength

The macroscale experiment test provides the data for the analysis of averaged (homogenized) response of a PPMC coupon with heterogeneous platelet meso-structure. The average Lagrangian strains in the loading x_1-direction, $\bar{\epsilon}_{11}(\Omega)$, determined by the DIC analysis on the front face of a coupon were plotted against effective tensile stress, $\bar{\sigma}_{11}$, to characterize the effective global and local response of a composite coupon. Average strains, $\bar{\epsilon}_{11}(\Omega)$, were extracted over a rectangular region of interest (ROI), Ω, of a specified size:

$$\bar{\epsilon}_{11}(\Omega) = \frac{1}{\Omega} \iint_{(x_1,x_2)\in\Omega} \epsilon_{11}(x_1, x_2)\, dx_1 dx_2 \tag{1}$$

Effective engineering stress $\bar{\sigma}_{11}$ was calculated by dividing the reaction force by the coupon average cross-sectional area. Specimen global average strain, $\bar{\epsilon}_{11}(\Omega^*)$, was calculated over the entire coupon speckled surface (5 in × 1 in ROI $\Omega = \Omega^*$) and then the local average strains, $\bar{\epsilon}_{11}(\Omega_i)$, were determined over 1 in × 1 in regions along the specimen length (ROI $\Omega = \Omega_i$, i = 1–4), see Fig. 3(a). Experimentally measured global, $\bar{E}_{11}(\Omega^*)$, and local, $\bar{E}_{11}(\Omega_i)$, effective tensile moduli of the composite coupons were calculated from the average strains over the large (Ω^*) and small (Ω_i) polygonal gage areas, respectively. The effective moduli were evaluated over the strain interval of 100–3500 με (0.01%–0.35%) for $[0^\circ/\pm 45^\circ/90^\circ_{1/2}]_s$-coupons and over the strain interval of 100–2000 με (0.01%–0.2%) for stochastic PPMC coupons as the slope of the corresponding stress-strain curves. The measured elastic moduli are summarized in Fig. 4(a). The different size of strain regions was used to understand how the local meso-scale morphology variability translates into the variability of effective PPMC modulus.

Stochastic morphology in PPMC coupons with uncontrolled meso-structure can produce significant inter- and intra-coupon deformation variability. Effective composite properties vary from one coupon to another and within the same coupon due to the local morphological dissimilarities, specifically the details of stochastic orientation state and platelets overlap. This is because of the lack of scale separation between the 25.4 mm × 25 mm × t domain size and 12.7 × 12.7 mm platelets, as stochastic meso-morphology can vary drastically due to a finite

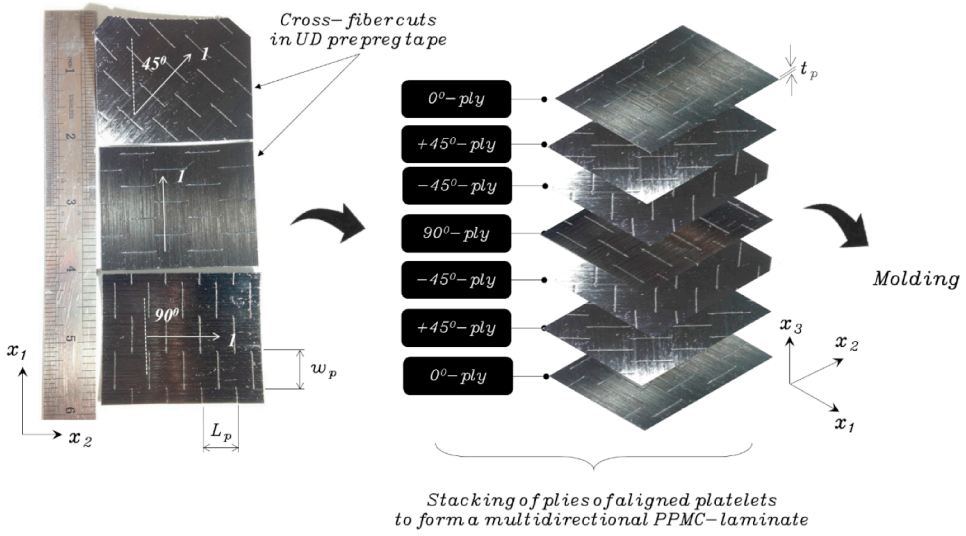

(a)

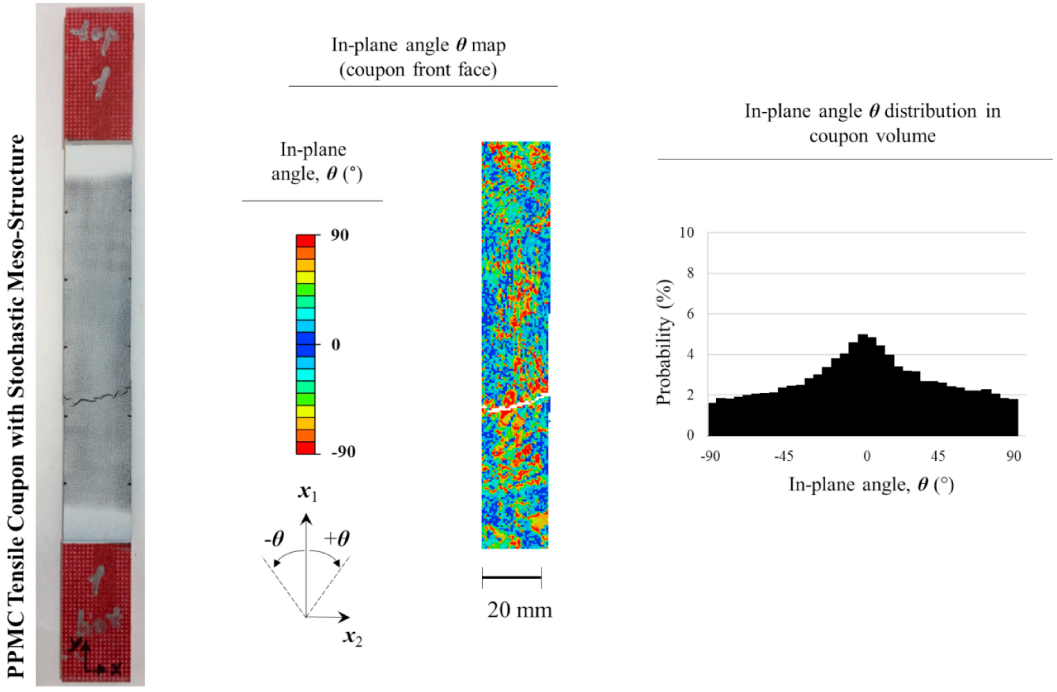

(b)

Fig. 2. (a) Manufacturing of a PPMC for the deterministic (controlled) orientation state: $[0/\pm 45/90_{1/2}]_s$ PPMC-laminate; (b) Analysis of orientation state in a PPMC coupon with stochastic meso-structure.

number of platelets within a domain. Fig. 2(b) shows an example of stochastic orientation state in a PPMC coupon with uncontrolled meso-structure, where the orientation analysis of coupon CT-scan images was performed with gradient based method as previously reported in Ref. [25]. Stochastic meso-scale morphology fluctuations are reflected in the heterogeneous coupon surface strains $\epsilon_{11}(x_1, x_2)$ observed with DIC, where significant gradients between the high and low strain regions can be seen in Fig. 3(a). The effect of dissimilarity of orientation states in stochastic uncontrolled morphologies can be seen in both local and global measures of coupons stiffness. The effective local stiffness $\bar{E}_{11}(\Omega_i)$ between five coupons had an average value of 31.7 GPa with 22.7% coefficient of variation (cov), while the effective global stiffness $\bar{E}_{11}(\Omega^*)$ between five coupons has an average of 30.9GPa with cov. 12.2%, see Fig. 4(a).

Morphology control results in a relatively regular pattern of the axial strain field $\epsilon_{11}(x_1, x_2)$ on the surfaces of $[0^\circ/\pm 45^\circ/90^\circ_{1/2}]_s$ coupons, especially as compared to the coupons with stochastic orientation strain, see Fig. 3(a). The underlying geometrical pattern of PPMC meso-structure can be recognized from the axial strain distribution with strain concentration seen at the platelet ends, meaning high strain is seen in Fig. 3(a) at regular intervals corresponding to the platelet length over the distances corresponding to the platelet width. Engineered morphology with controlled orientation state in $[0^\circ/\pm 45^\circ/90^\circ_{1/2}]_s$-coupons provides for a substantial reduction in the variability of

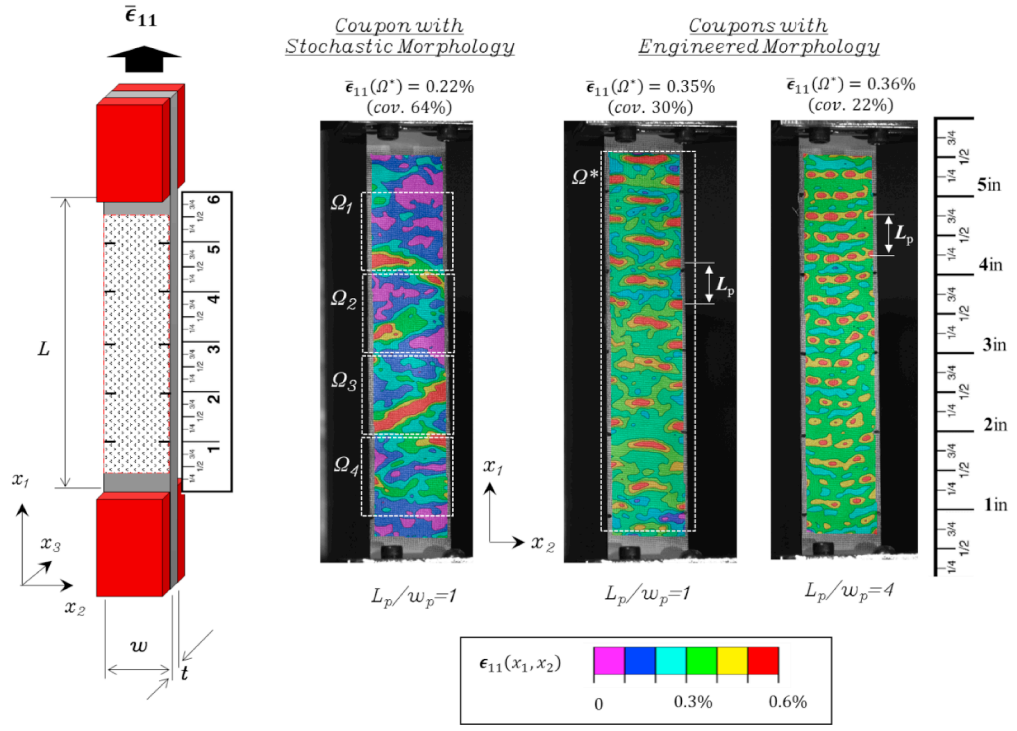

(a)

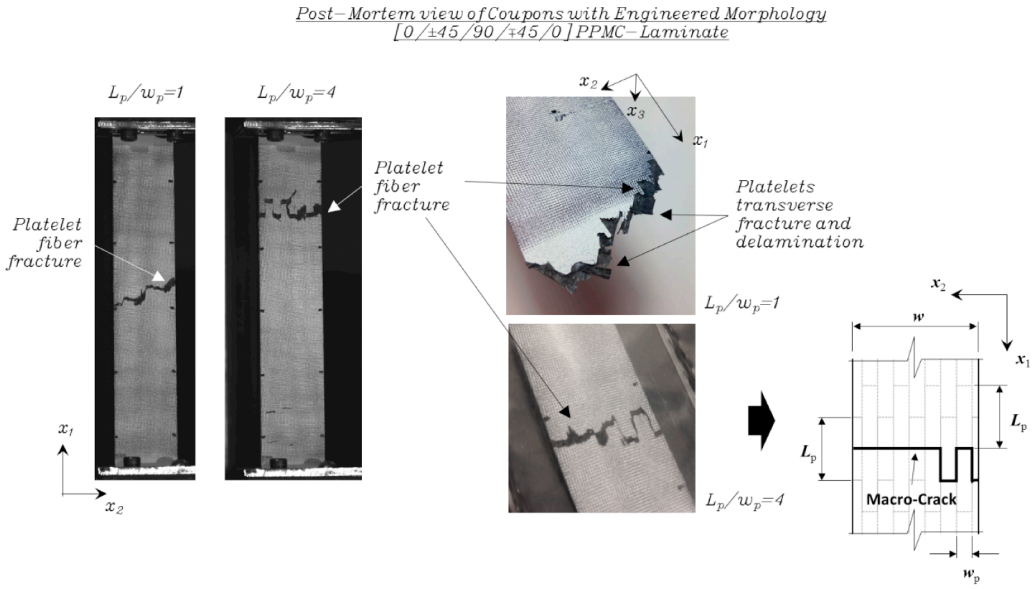

(b)

Fig. 3. (a) DIC measured tensile strain distribution, ϵ_{11} (x_1, x_2), on the faces of coupons with stochastic and engineered meso-morphologies; (b) Fractured tensile coupons of engineered morphology.

effective mechanical properties. This is because the morphological dissimilarities are reduced (but not eliminated) between these coupons since the orientation variability is nominally revoked, while the platelet local overlap variability is retained. The effective local stiffness $\bar{E}_{11}(\Omega_i)$ between five coupons with $L_p/w_p = 1$ and $L_p/w_p = 4$ had average values of 47.8 GPa (cov. 4.14%) and 49.6 GPa (cov. 3.07%), respectively. The global coupon stiffness $\bar{E}_{11}(\Omega^*)$ had an average value of 47.6 GPa (cov. 2.2%) for platelets with $L_p/w_p = 1$ and 49.9 GPa (cov. 1.34%) for platelets with $L_p/w_p = 4$, see Fig. 4(a).

The average effective strength is improved from 119 MPa for the PPMC coupons with stochastic meso-structure to 303 MPa for engineered morphology for the same 0.5 × 0.5 in platelet size and nearly the same coupon thickness, while the strength variability decreases from 13.8% to 6.01%, as reported in Fig. 4(b). This is due to a designed orientation state and ordered meso-structure, wherein any out-of-plane orientations are removed. Orientation state control reduces the number of stochastic "weak spots" thus contributing to mitigated variability of properties. A PPMC system derives its functions through a hierarchical organization of its structural elements (platelets). Hartmann and Schwieger [26] postulated that hierarchy is always related to such properties as material stiffness and strength. A repeatable pattern of geometrical arrangement of platelets in a composite

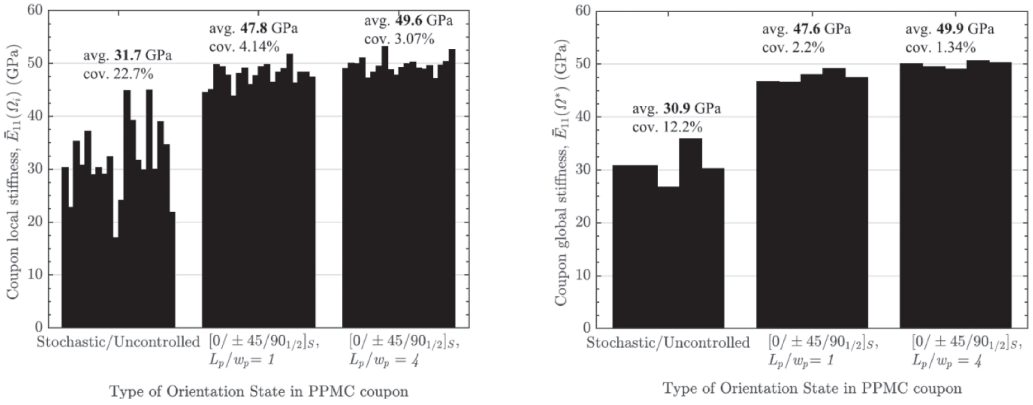

(a)

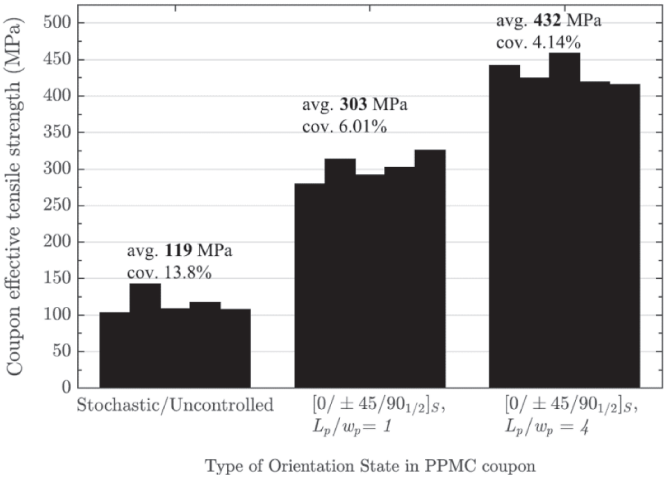

(b)

Fig. 4. Experimental tensile properties of prepreg platelet molded composite systems with uncontrolled morphology ($L_p/w_p = 1$) and engineered morphology ($L_p/w_p = 1$, $L_p/w_p = 4$): (a) effective elastic modulus $\bar{E}_{11}$ measured from small Ω_i (left) and large Ω^* (right) ROIs; (b) effective strength.

system stipulates an improved hierarchical organization of composite meso-structure. Planar overlap regions in ordered PPMC morphology allow platelets to build more in-plane stresses and lower the inter-laminar (platelet-to-platelet) stresses compared to complex curved overlaps between platelets in a stochastic PPMC. Therefore, an ordered (geometrically "simpler") material morphology enhances stress transfer between platelets and grants improved effective performance characteristics to the material system as compared to the case of a lower level of hierarchical organization in a stochastic morphology.

Fig. 4(b) reports the effective tensile strength of $[0^\circ/\pm 45^\circ/90^\circ_{1/2}]_s$-coupons for both platelet length-to-width ratios, L_p/w_p, of 1 and 4. It appeared that a narrower (0.5 × 0.125 in) platelet provided for a substantial improvement to effective strength as compared to a square (0.5 × 0.5 in) platelet, from 303 MPa (cov. 6.01%) to 432 MPa (cov. 4.14%). A heterogeneous composite system of many platelets is a highly redundant structural system, meaning some of its elements may fail forcing the redistribution of loads in the system among the undamaged components such that the entire system may continue to sustain the applied load. The narrower platelet implies a greater number of elements in the composite system. Upon loading a coupon during testing, early damage is registered as a number of audible "pings" and "tings" emanating before the ultimate strength is reached. The ultimate strength, i.e. the stress at macroscopic/ultimate failure, is recorded as an abrupt load drop. First audible events corresponding to initial failure occur at about the same loading levels (~150 MPa) for both $[0^\circ/\pm 45^\circ/90^\circ_{1/2}]_s$-coupons of platelets with $L_p/w_p = 1$ and 4. With more platelet elements, the system of platelets with $L_p/w_p = 4$ had more structural redundancy and could sustain a longer damage evolution before reaching its ultimate strength.

Fig. 3(b) shows the complex topology of a macroscopic crack after coupon ultimate failure. The macroscopic crack appears as a poly-surface, a connected sequence of individual surfaces, which are local meso-scale fractures disrupting the continuity of the PPMC meso-structure. The known geometrical arrangement of platelets can help identify the meso-scale failure modes involved. The outer layers in a $[0/\pm 45/90_{1/2}]_s$ coupon have uniformly staggered platelets aligned with the global x_1-direction, as shown in Fig. 2 and in the schematics in Fig. 3(b). Examination of the macro crack "serrated" profile, along with knowledge of the platelet staggering in the coupon outer layer, leads to the conclusion that the macro-crack does not fully follow the pattern of platelet edge discontinuities, which implies that fracture goes across the platelet interior at certain locations. Next, since the macro-crack does not appear to be a straight cut through the coupon thickness, delaminations between platelets are present. Therefore, as could be anticipated, the

observed damage modes include fiber fracture (within a platelet), platelet splitting along the fibers and delamination between platelets, signifying that meso-scale damage does not occur in isolated modes in a PPMC. Damage modes in a PPMC are interactive due to complex nature of damage initiation and growth. Engagement of various damage modes promotes further energy absorption by composite during the progressive damage growth, while the meso-structure continues to carry the load in the presence of damage.

3. Mesoscopic computational analysis of a composite system with multi-directional planar layers of staggered platelets

The following section describes the development and application of the computational model to predict the PPMC-laminate macroscopic tensile properties from the composite meso-structure and platelet material properties. The model validation is performed by comparison of simulated composite macro-response with experimental data from tensile coupons described in Section 2.

3.1. Formulation of the computational model with "Windowing" approach and direct numerical homogenization

The studied laminated composite system (PPMC-laminate) consists of multi-directional layers of aligned and staggered prepreg platelets with length, L_p and width, w_p. The platelet thickness, t_p, is constant and indicates the ply thickness. A global coordinate system (x_1, x_2, x_3) is assigned such that the x_1x_2-plane is coplanar with the layers of platelets and x_3 is the laminate thickness direction, as shown in Fig. 5. Each layer of platelets is identified by a stacking angle, θ, measured between the platelet fiber direction "*1*" and the global x_1-axis. The lamination sequence $[\theta_1/\theta_2/\theta_3]$ reads as in the traditional continuous fiber laminates starting with the first ply in lay-up.

The analysis of a platelet-arrayed composite system is conducted at the meso-scale to incorporate the properties and architectural arrangement of individual platelets. The analysis objective is to bridge the meso- and macro- length scales in a PPMC-laminate and derive the composite macro response to quasi-static uniaxial tensile loading. This was accomplished by applying the macroscopic strain $\bar{\epsilon}_{11}$ to the composite system and calculation of the corresponding stress $\bar{\sigma}_{11}(\bar{\epsilon}_{11})$. Homogenization (up-scaling, "coarse graining" by Böhm [27]) allows one to deduce the overall properties at some larger length scale ("macro-scale", or "coarse grained" scale [27]) from smaller length scale ("fine grained" [27]) information, i.e. from the known constitutive laws of the inhomogeneous system sub-scale phases and their geometrical arrangement. The overall properties of a material system influenced by its underlying sub-scale quantities are called effective (or homogenized) properties. The most straightforward application of homogenization analysis is for virtual material characterization. In practice, effective properties are averaged over a certain sample volume V of the heterogeneous system. This sample volume V must be sufficiently large to contain all necessary information about discrete morphology to describe the composite up-scale behavior. The complex overlap distribution of misaligned platelets does not allow the definition of a periodic sample volume (a "unit cell" [28]). Therefore, a non-periodic sample volume for homogenization is herein termed a "mesoscopic test window" or "observation window" [27] rather than a representative volume element (RVE) following the established semantics. Although, the terms "non-periodic RVE" or just an "RVE" are sometimes also used for a sample of a non-ergodic material. The general scheme of the first-order direct computational homogenization was detailed by Suquet [29]. It requires several steps: (*i*) the definition of a "computational window" or an RVE, whichever exists for a considered heterogeneous system, with main inputs being the geometrical arrangement and specified constitutive behavior of composite elements; (*ii*) choice of appropriate boundary conditions; (*iii*) analysis of local stress and strain fields; and (*iv*) obtaining the relationship between the macroscopic input, $\bar{\epsilon}_{11}$, and output, $\bar{\sigma}_{11}$, variables.

Platelets in different layers have different extensional stiffness in the x_1-x_2-x_3 coordinate system due to their fiber orientations. When system is loaded, platelets begin to interact. Any platelet experiences a biaxial state of stress in the x_1x_2 plane when its fiber direction makes an angle with the loading direction even in the case of a unidirectional loading, except for the boundary region existing near the platelets edges (the geometric/stiffness discontinuities). The boundary regions within each

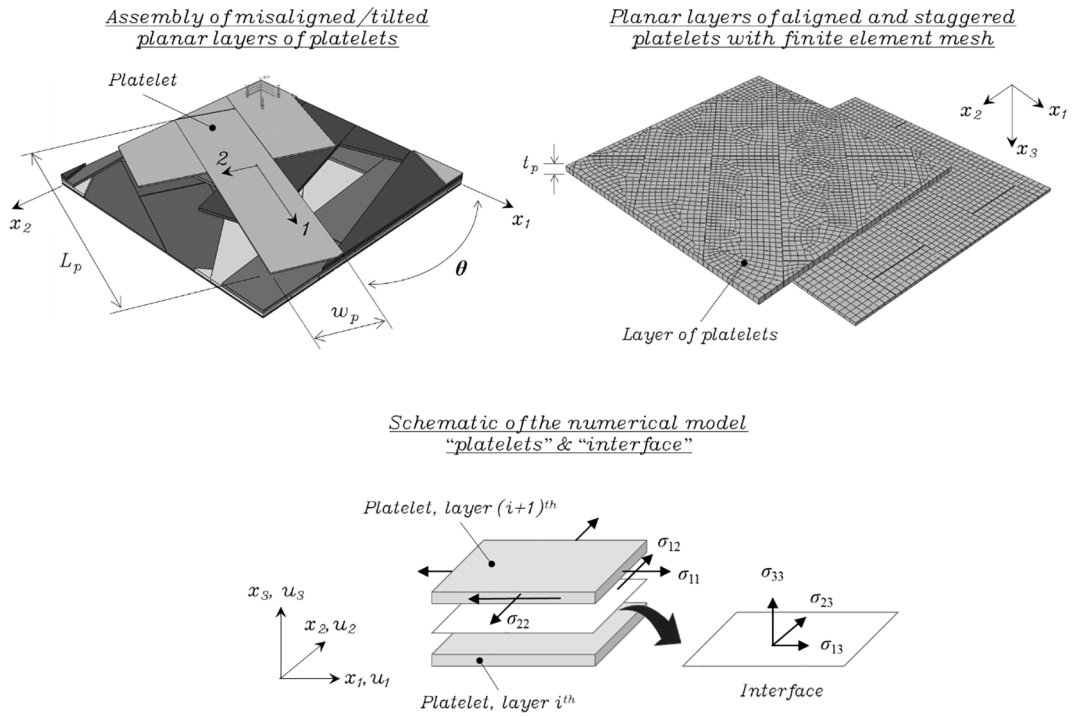

Fig. 5. Schematic of the computational model of a composite system of misaligned planar layers of aligned and staggered platelets.

platelet are the regions wherein stress transfer between adjacent platelets is accomplished through the action of out-of-plane stresses. This means that the state of stress in the boundary layers is three-dimensional. Out-of-plane stresses are caused by the mismatch of material properties in the bonded adjacent platelets and arise even when the platelet-based composite system is subjected to in-plane loading. Therefore, the three-dimensional stress transfer must be ensured in the computational model of a PPMC. The platelets are assumed to carry the in-plane stress components (σ_{11}, σ_{22}, σ_{12}), since the platelet thickness (t_p) is taken to be much smaller than its planar dimensions (L_p, w_p). The stress transfer between platelets is assumed to be entirely through the platelet-to-platelet interface in overlap regions. The interface is assumed to transmit out-of-plane transverse shear (σ_{13}, σ_{23}) and normal peel stress (σ_{33}) between platelets. The assumed stress carrying capacity of composite elements is schematically shown in Fig. 5. For simplicity, the edges of the platelets were assumed to be traction free. This assumption corresponds to Cox's shear-lag model [30] for a short fiber composite. In all simulations, the distance between the discontinuous edges of the platelets was assumed 50 μm. The effect of the spacing between platelets was previously studied for the composite array of aligned staggered platelets [31].

3.2. Finite element implementation of the progressive failure analysis

Herein, progressive failure analysis (PFA) is used to simulate the damage accumulation and predict the ultimate load carrying capacity of a PPMC-laminate. The progressive failure model is a combination of intra- and inter-platelet failure criteria and post-failure degradation rules. The failure analysis is based on the calculation of the platelet and platelet-to-platelet level stresses which are then compared to the assigned strength values by applying corresponding failure criteria. The failure criteria indicate whether local failure occurs and what is the mode of failure. The local damaged areas are then characterized with impaired (degraded) constituent material properties. Once an element with the combination of stresses that result in a particular failure mode is identified, the corresponding stiffness of that element is reduced such that a weakened/damaged element is no longer able to support as much load as the undamaged elements surrounding it. The internal loads are then redistributed around the weakened element into the full stiffness (undamaged) elements, which in turn causes the yet undamaged elements to carry a higher loading than they would if a weakened element would not have failed. This causes new elements to fail and this process continues until enough elements fail that the entire structure is weakened to the point that it cannot support an increase in the applied load. The incorporation of the progressive damage model in the finite element analysis allows for the influence of various types of damage on the failure strength of a composite system.

Meso-scale constitutive response of a platelet is described with ABAQUS/Standard's (Implicit) built-in anisotropic continuum damage mechanics (CDM) model [32,23]. The damaged microstructure of a platelet leads to a degradation of its stiffness observed on the meso-scale, where the platelet is treated as an orthotropic homogenized continuum. CDM is a constitutive theory for a homogeneous medium that describes the progressive loss of material integrity by a set of continuous damage variables. Therefore, the platelet orthotropic in-plane damage which is the result of the biaxial state of stress, is modeled by the evolution of several internal variables, d_{ij}, which control the systematic reduction of the orthotropic compliance matrix of the material, as given by Eq. (2):

$$\begin{Bmatrix} \epsilon_{11} \\ \epsilon_{22} \\ 2\,\epsilon_{12} \end{Bmatrix} = \boldsymbol{H}(\boldsymbol{d}) \begin{Bmatrix} \sigma_{11} \\ \sigma_{22} \\ \sigma_{12} \end{Bmatrix} + \Delta T \begin{Bmatrix} \alpha_{11} \\ \alpha_{22} \\ \alpha_{12} \end{Bmatrix}, \tag{2}$$

where ϵ_{ij} and σ_{11} are the mechanical strain and stress, respectively; ΔT is the temperature differential; α_{ij} are the coefficients of thermal expansion; $\boldsymbol{H}(\boldsymbol{d})$ is the damaged compliance matrix of a platelet and $\boldsymbol{d}$ is the vector of damage variables, both are given in Eq. (3). Herein, d_{11} reflects the damage in the fiber direction, d_{22} accounts for the damage in the second preferential direction, and d_{12} is the parameter for in-plane shear damage that depends on the damage variables d_{11} and d_{22} [32]. The damage variables are monotonically increasing functions in the range of $0 \le d_{ij} \le 1$, with $d_{ij} = 0 (i, j = 1–2)$ corresponding to the initial undamaged material and $d_{ij} = 1 (i, j = 1–2)$ representing a state of complete loss of integrity with no stress can be transferred. The material elastic constants in Eq. (3) correspond to the platelet precursor UD CF prepreg tape.

$$\boldsymbol{H}(\boldsymbol{d}) = \begin{bmatrix} \frac{1}{(1-d_{11})E_{11}} & -\frac{\nu_{21}}{E_{22}} & 0 \\ -\frac{\nu_{12}}{E_{11}} & \frac{1}{(1-d_{22})E_{22}} & 0 \\ 0 & 0 & \frac{1}{(1-d_{12})G_{12}} \end{bmatrix}, \boldsymbol{d} = \begin{Bmatrix} d_{11} \\ d_{22} \\ d_{12} \end{Bmatrix} \tag{3}$$

The initiation of damage is governed by the effective stress components $\hat{\sigma}_{ij}$ through Hashin's criteria [33] shown in Eqs. (4):

Fiber tension ($\hat{\sigma}_{11} > 0$): $$\left(\frac{\hat{\sigma}_{11}}{X^T}\right)^2 = 1 \tag{4a}$$

Fiber compression ($\hat{\sigma}_{11} < 0$): $$\left(\frac{\hat{\sigma}_{11}}{X^C}\right)^2 = 1 \tag{4b}$$

Transverse tension ($\hat{\sigma}_{22} > 0$): $$\left(\frac{\hat{\sigma}_{22}}{Y^T}\right)^2 + \left(\frac{\hat{\sigma}_{12}}{S_{12}}\right)^2 = 1 \tag{4c}$$

Transverse compression ($\hat{\sigma}_{22} < 0$): $$\left(\frac{\hat{\sigma}_{22}}{2S_{23}}\right)^2 + \left[\left(\frac{Y^C}{2S_{23}}\right)^2 - 1\right]\frac{\hat{\sigma}_{22}}{Y^C} + \left(\frac{\hat{\sigma}_{12}}{S_{12}}\right)^2 = 1 \tag{4d}$$

After the failure has been initiated by satisfying the given failure criteria, the corresponding stresses are degraded following a linear softening law. The evolution of damage is defined in terms of the fracture energy dissipated during the damage process [34], G_C, and defined for each failure mode. In the present investigation numerical values for G_c were adopted from [32]. The longitudinal tensile and compressive fracture energy was assumed 12.5 kJ/m^2, while the transverse tensile and compressive fracture energy was taken as 1 kJ/m^2. The thermal and mechanical properties used in Eqs. (2)–(4) are summarized in Table 1 for the AS4/PEKK UD CF tape [35].

Delamination of platelets was idealized with an interfacial damage model implemented through the surface-based cohesive behavior in ABAQUS/Standard (Implicit). Every layer of platelets was modeled as a separate part in ABAQUS, with each part meshed dominantly with

Table 1
Material properties for the AS4/PEKK UD tape used in the computational analysis.

Material Property	Numerical value
Longitudinal modulus, E_{11} [GPa]	130.656
Transverse modulus, E_{22} [GPa]	9.583
Shear modulus, G_{12} [GPa]	5.7
Shear modulus, G_{23} [GPa]	4.0
Poisson's ratios, ν_{12}	0.32
Poisson's ratio, ν_{23}	0.45
Longitudinal coefficient of thermal expansion, α_{11} [με/°C]	1
Transverse coefficient of thermal expansion, α_{22} [με/°C]	25
Longitudinal tensile strength, X_t [MPa]	2157
Longitudinal compressive strength, X_c [MPa]	1270
Transverse tensile strength, Y_t [MPa]	78
Transverse compressive strength, Y_c [MPa]	113
Longitudinal shear strength, $S_{12} = S_{13}$ [MPa]	109
Transverse shear strength, S_{23} [MPa]	86

SC8R finite elements, an 8-node hexahedron continuum shell with reduced integration. Because of the geometrical complexity of the layers of tilted platelets, SC6R, a 6-node triangular in-plane continuum shell wedges were used as necessary. Surface-to-surface contact with frictionless tangential, hard normal and cohesive behaviors was assigned between the individual layers of platelets. It was assumed that the upper surface of each layer was a "master", while the bottom surface of a layer was a "slave" in contact interactions. Surface-based cohesive behavior (ABAQUS) is defined for contact pairs in Abaqus/Standard and provides a simplified way to model cohesive connections with negligibly small interface thickness using the traction-separation constitutive model, which relates the contact (interface) tractions, σ_{i3}, to the contact separations, $\delta_i = \Delta u_i$ $(i = 1, 3)$, between the adjacent surfaces:

$$\begin{Bmatrix} \sigma_{13} \\ \sigma_{23} \\ \sigma_{33} \end{Bmatrix} = \begin{bmatrix} (1-d)k_1^0 & 0 & 0 \\ 0 & (1-d)k_2^0 & 0 \\ 0 & 0 & (1-d)k_3^0 \end{bmatrix} \begin{Bmatrix} \delta_1 \\ \delta_2 \\ \delta_3 \end{Bmatrix} \tag{5}$$

In Eq. (5), $k_i^0 = 1(10^6)\,\frac{\text{MPa}}{\text{mm}}$ $(i = 1\text{–}3)$ is the initial interface stiffness; d is the isotropic damage variable, with $d = 0$ corresponding to intact interface and $d = 1$ corresponding to a propagated delamination. A stress-based quadratic criterion was selected [36] for the initiation of dis-bonding between platelets, Eq. (6):

$$\left(\frac{\langle \sigma_{33} \rangle}{N_{max}}\right)^2 + \left(\frac{\sigma_{13}}{S_{max}}\right)^2 + \left(\frac{\sigma_{23}}{T_{max}}\right)^2 = 1 \tag{6}$$

The numerical values of cohesive strengths used in the simulations were: $N_{\max} = 50$ MPa, $S_{\max} = T_{\max} = 70$ MPa. For the propagation of delamination, a power-law fracture mechanics-based criterion was used [37], Eq. (7):

$$\frac{G_I}{G_{IC}} + \frac{G_{II}}{G_{IIC}} + \frac{G_{III}}{G_{IIIC}} = 1 \tag{7}$$

where G_{I}, G_{II}, and G_{III} are the work done by the tractions in the normal and shear modes, respectively. Quantities with subscript "C" denote the critical strain energy release rates corresponding to each fracture mode ($G_{IIC} = G_{IIIC}$) and are taken as the precursor UD CF prepreg tape delamination fracture toughness values (Table 2). Herein, interfacial properties are taken as independent of the fiber orientation in the adjacent plies, meaning the assumption is made that the delamination fracture toughness values for aligned material should be sufficiently representative to rank the overall behavior of laminates with complex stacking sequences. Although, there were evidences reported in the literature (e.g. Gong et al. [38] for more details) that delamination resistance may vary as a function of laminate stacking sequence, adjacent fiber orientation and specimen geometry; that is, in general the fracture toughness may depend on the fracture surface morphology if a crack is initiated in a θ_1/θ_2 interface.

Mathematically expressed, the formulae and laws that govern surface-based cohesive behavior are similar to those used for cohesive elements with traction-separation behavior. However, from the finite element implementation and analysis point of view, the damage in surface-based cohesive behavior is an interaction property, not a material property; tractions and separations are interpreted differently for cohesive elements and cohesive surface.

The viscous regularization method [39,40], implemented in ABAQUS/Standard, was used to reduce damage localization and improve numerical convergence of the solution. The following stabilizing parameters were used for the damage model of a platelet: viscosity coefficient for the damage variable d_1, $\eta = 1(1\,0^{-3})1/\text{s}$; viscosity coefficients for the damage variable d_2, $\eta = 5(1\,0^{-3})1/\text{s}$. These numbers were adopted from [32]. Viscous regularization of interface damage variable was used with the viscosity coefficient of $\eta = 2(1\,0^{-4})1/\text{s}$.

Periodic boundary conditions [29] in the finite element analysis were applied where necessary as nodal displacement constraint equations on opposite boundary faces of a computational window:

$$u_i^{k+}(x_1, x_2, x_3) - u_i^{k-}(x_1, x_2, x_3) = \bar{\epsilon}_{ij}\,(x_j^{k+} - x_j^{k-}) \tag{8}$$

where superscripts "$k+$" and "$k-$" indicate the positive and negative directions along the x_{k} direction, respectively, and $\bar{\epsilon}_{ij}$ is the applied macroscopic strain. The constraints defined in Eq. (8) were defined for every pair of matching (if possible) or nearest (otherwise) nodes. They specify the displacement differences between the opposite boundary faces of a computational volume according to the applied macroscopic strain and the distance between the faces.

3.3. Model validation

As pointed out by Henninger et al. [41], confidence in computational simulations is possible if the mathematical foundation of the model is verified and the simulated results are validated against the sound experimental data. The available physical observations are key to any validation assessment, argues Council [42]. The emphasis of this section is on external validation [43] as the comparison of simulated and real data of macro stress-strain response and failure modes.

A sample morphology of a [0/ ± 45/90/∓45/0] PPMC-laminate is considered for two platelet sizes, L_{p}xw_{p}, 12.7 × 12.7 mm and 12.7 × 3.175 mm, corresponding to $L_{\text{p}}/w_{\text{p}} = 1$ and 4, respectively. The platelet thickness, t_{p}, is 0.12 mm. The non-periodic RVE (computational window) dimensions along the global x_1 and x_2 directions are 25.4 × 25.4 mm (1 × 1 in), while the RVE thickness is $7t_{\text{p}}$. Periodic boundary conditions are only applied on the x_1-faces with x_1 being the loading direction. The described computational models are assembled to make a comparison with experimental results from the $[0^0/\pm 45^0/\bar{90}^0]_s$-tensile coupons from Section 2.

The simulated effective (macroscopic) response of a tensile sample (RVE) is characterized with engineering strain, $\bar{\epsilon}_{11}$, and stress, $\bar{\sigma}_{11}$, defined as the fraction of loading displacement to initial gage length and reaction force to the average cross-sectional area of an RVE, respectively. Acceptable correlation between the simulation and experimental macro stress-strain curves $\bar{\sigma}_{11}(\bar{\epsilon}_{11})$ from uniform tension tests for both platelet sizes, $L_{\text{p}}/w_{\text{p}} = 1$ and 4, in a [0/ ± 45/90/∓45/0]-laminate is shown in Fig. 6. Experimental macro strain $\bar{\epsilon}_{11}$ (Ω^*) is calculated by averaging the DIC-measured surface tensile strains over the 5 × 1 in gage region Ω^*.

The failure mechanisms are rather complex due to inhomogeneous composition of platelet-arrayed system with distinctly different platelet orientations and, consequently, properties. A number of different failure modes are present. Computational results provide insight into the different load-deformation stages exhibited by the platelet mesostructure during axial loading. After some critical loading, the initial linear global response (both simulated and experimental) is followed by a non-linear segment of the macroscopic stress-strain curve. This is when experimental tensile coupons begin emanating "pings" and "tings", thereby indicating the initiation of damage growth. The composite effective stiffness degradation with applied strain, $\bar{C}_{11}(\bar{\epsilon}_{11})$, is a result of the progressive damage development. The damage mechanisms in a structure made of platelets begin with platelet transverse cracking near the edges of adjacent platelets. Multiple transverse cracks are generated in platelets at the lower applied strain prior to ultimate

Table 2
Fracture properties for the AS4/PEKK UD tape used in the computational analysis.

Material Property	Numerical value
Mode I delamination fracture toughness, G_{IC} [kJ/m^2]	1.436
Mode II delamination fracture toughness, G_{IIC} [kJ/m^2]	2.380

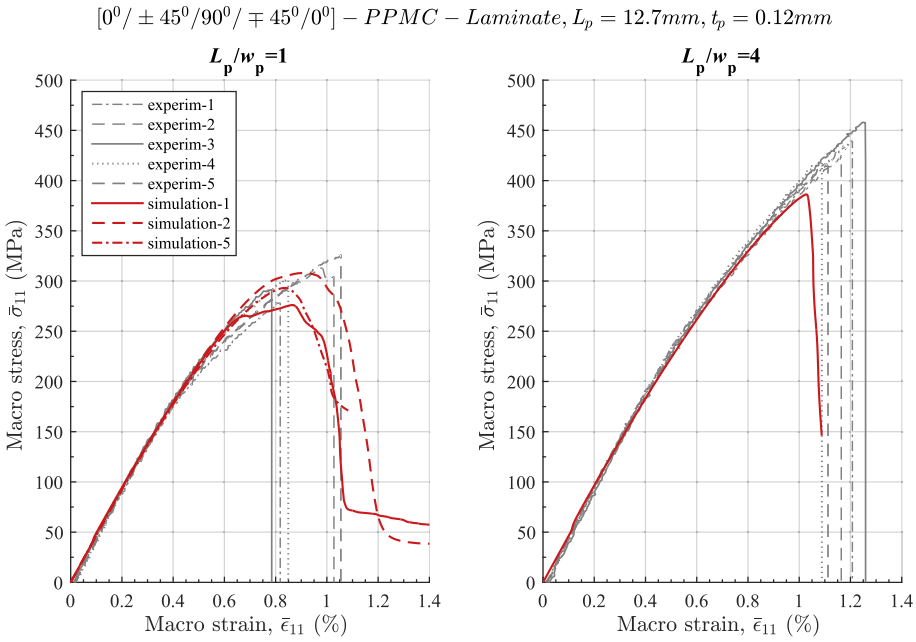

Fig. 6. Simulated vs experimental effective stress-strain curves of a [0/ ± 45/90/∓45/0] PPMC-laminate with two length-to-width ratios: $L_p/w_p = 1$ (left) and $L_p/w_p = 4$ (right).

failure. Moreover, the first damage also includes local delaminations from the interlaminar stresses concentrated near platelet edges. Delamination is detrimental since it disrupts load sharing between adjacent debonded platelets. The simulated damage evolution correlates with the in-situ observation of the damage process previously reported by Taketa et al. [13]. The composite system can carry considerable load after initial failure by redistributing the stresses among the remaining undamaged components as the locally damaged spots are gradually unloaded. The initially small-localized damaged zones grow and coalesce with further applied load to form a macroscopic crack. The system reaches its ultimate strength then and loses its load-bearing capacity. The simulation indicated platelet fiber breakage in some of the zero-degree platelets at the system ultimate strength, and agrees with what was observed experimentally. The platelet fractured fibers can be seen in Fig. 3(b) where it is indicated by the disrupted pattern of zero-degree platelets. In general, the macroscopic crack may have a complex topology appropriate to a particular failure mode of the system including combinations of splits in the fiber direction and fractures perpendicular to the fiber direction in the platelets, and delamination between platelets.

4. Theoretical analysis of the structure-property relationship in a PPMC-laminate

Modeling of a platelet-based composite system allows simulation of its mechanical behavior, which aids in defining the composite structure-property relationship. Effect of platelet length-to-thickness and length-to-width ratio on composite tensile strength is investigated. The variability of tensile properties caused by the overlap distribution of platelets in a PPMC-laminate with a deterministic orientation state is considered. The effect of thermal-residual stresses on the ultimate strength of a PPMC-laminate is discussed.

4.1. Effect of meso-scale thermal-residual stress on tensile strength of a PPMC laminate

A thermo-elastic analysis was developed to determine the thermal residual stresses in a multi-directional PPMC. The model assumes that the stress-free temperature is defined as the glass transition temperature (T_g). It is assumed that a virtual sample (RVE) of the PPMC laminate is subjected to a uniform temperature differential of $\Delta T = -135\,^{\circ}C$ for the thermal-residual stress analysis, for $T_g = 160\,^{\circ}C$ and room temperature is 25 °C. The RVE is subsequently tested in-silico in tension by applying the mechanical strain until the ultimate failure event occurs. The considered PPMC-laminate is $[0/\pm 45/90_{1/2}]_s$ having platelets with dimensions of $L_p \times w_p \times t_p = 12.7 \times 12.7 \times 0.12$ mm. The in-plane dimensions of the 0.84 mm-thick ($7t_p$) RVE are 25.4 × 25.4 mm.

Thermal residual stresses in a multi-directional PPMC laminate appear at both micro- and meso-scales. Micro-residual stresses originate from the mismatch of thermal expansion coefficients (CTE) and moduli between the fibers and the resin, the micro-constituents of a platelet. The thermal residual stresses in the meso-scale of a PPMC laminate are developed from the mismatched CTEs and mechanical properties of plies with different fiber directions. As the meso-scale computational model of a PPMC-laminate proposed in Section 3.2 considers platelets as homogeneous orthotropic material, it allows to evaluate the locked-in in-platelet (meso-scale) thermal residual stresses caused by the cool down (to the room temperature) during the manufacturing stage and investigate their effect on the composite ultimate failure strength during subsequent tensile loading. The AS4/PEKK carbon-fiber/thermoplastic PPMC-laminate is processed at its melt temperature (340 °C) [35] and further cooled-down to the room temperature. As the temperature decreases, the crystalline portion of the semi-crystalline PEKK undergoes crystallization at 280 °C, while the amorphous portion experiences a rubbery stage and then reaches its $T_g = 160\,^{\circ}C$, and turns into a glassy (solid) form. The Dynamic Mechanical Analysis (DMA) (Fig. A1, Appendix) shows that neat PEKK resin has a low storage modulus above the glass transition temperature. Previously, based on the similar DMA data, Tzeng [44] suggested that the matrix dominated properties such as the transverse E_{22} and shear G_{12} moduli of a unidirectional continuous fiber lamina must be low at temperatures above the T_g, and accordingly the residual stresses resulting from these properties may be considered negligible in the temperature range above T_g. Similarly, Jeronimidis and Parkyn [45] concluded that about 75% of the residual stress level in the fiber-thermoplastic laminates builds up between the T_g and room temperature.

Meso-scale thermal-residual stresses in the $[0/\pm 45/90_{1/2}]_s$ PPMC-laminate are found to not have a substantial effect on the ultimate

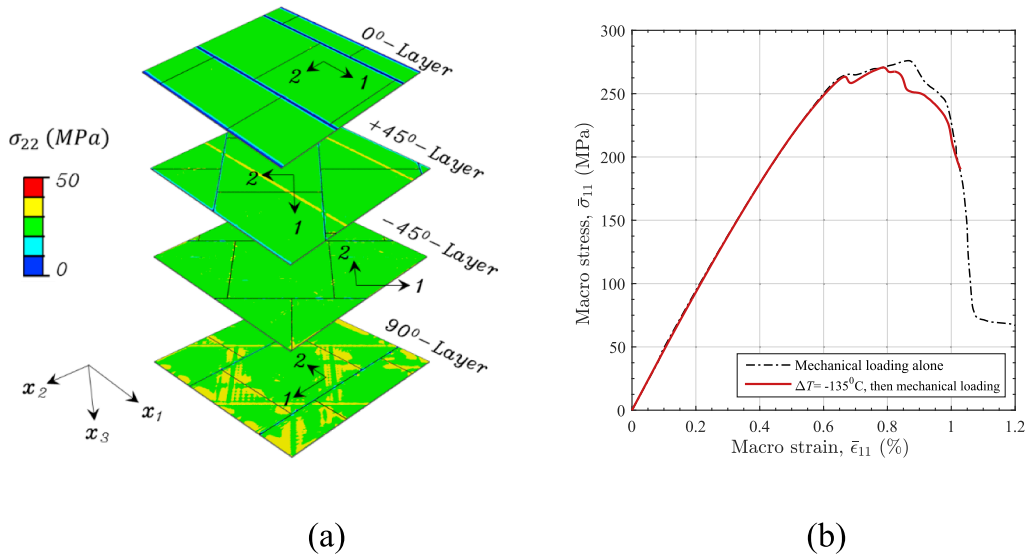

Fig. 7. Effect of thermal residual stresses on the effective tensile response of the $[0/\pm 45/90_{1/2}]_s$ PPMC-laminate, $L_p \times w_p \times t_p = 12.7 \times 12.7 \times 0.12$ mm: (a) in-platelet thermal-residual transverse stress σ_{22} from $\Delta T = -135\,^{\circ}C$; (b) effective stress-strain curves of a PPMC-laminate with and without thermal-residual stresses.

strength. The applied temperature differential $\Delta T = -135\,^{\circ}C$ results in the magnitude of in-platelet longitudinal σ_{11} and transverse σ_{22} stress of about -30 MPa and 30 MPa, respectively, thus producing no meso-scale damage according to the damage initiation criteria in Eq. (4) and material properties in Table 1. The distribution of thermal-residual transverse stress in the individual plies of the PPMC laminate is shown in Fig. 7(a). The progressive failure response of the PPMC-laminate is somewhat affected by the account of the thermal-residual stresses. Fig. 7(b) compares the effective tensile stress-strain curves of the PPMC-laminate with and without considering the thermal-residual stresses. The ultimate strength seems to be not affected substantially by the account of the thermal-residual stresses, being reduced from 276 MPa to 271 MPa (i.e. by less than 2%). Based on this conclusion, the thermal-residual stresses were not considered in the subsequent sections.

4.2. Effect of meso-structure geometry on variability of tensile properties of a PPMC laminate

A PPMC-laminate with a deterministically defined orientation state of plies of aligned staggered platelets exhibits a distribution of tensile stiffness and strength, as experimental data in Fig. 4 shows. During consolidation of a PPMC-laminate the local material flow may somewhat change the designed meso-structure. Acknowledging the existence of general experimental error, we hypothesize that a primary factor for variability of PPMC-laminate tensile properties is the overlap distribution between platelets from adjacent layers within individual samples of composite meso-structure, even for a fixed orientation state of the composite system and fixed staggering order of platelets within a layer. We justify this hypothesis by the simulation results further shown in this section, wherein only the meso-structure geometry is varied, while the orientation state and local material properties are deterministic and loading conditions are free of experimental error. It has been previously shown in a systematic way for a system of aligned platelets [31] that the overlap length between platelets plays an essential role in the load transfer mechanism, influencing the strength and failure modes. Local heterogeneity of PPMC-laminate morphology manifests itself in a similar fashion. Changed distribution of overlaps between platelets alters the stress fields in a PPMC-laminate, thus redefining the regions of high stress concentrations. Therefore, the variability of meso-structure geometry translates into the variability of composite effective tensile properties.

The effect of meso-structure geometry in a $[0/\pm 45/90_{1/2}]_s$ PPMC-laminate with platelet dimensions of $L_p \times w_p \times t_p = 12.7 \times 12.7 \times 0.12$ mm is considered. Five virtual samples (RVEs) of PPMC-laminate meso-structure are analyzed for tensile stiffness and strength. The RVE global in-plane dimensions were 25.4×25.4 mm and the thickness was 0.84 mm ($7t_p$). Ply morphology of several selected RVEs is shown in Fig. 8(a) along with post-mortem state of the RVEs. The macroscopic fracture is seen to be dependent on the local arrangement of platelets within an RVE. The effective-stress strain curves of the selected virtual meso-structure samples are shown in Fig. 6 where they can be compared to the experimental curves. The simulated effective tensile properties of a PPMC-laminate are summarized in Fig. 8(b), where the simulation and experimental results are compared. The simulated variability of tensile stiffness and strength of the PPMC-laminate caused by the variable overlap distribution between platelets seems to agree well with the observed variability of the experimental data: the experimental and simulation average stiffness and strength are 47.6 GPa (cov. 2.2%) vs 46.7 GPa (cov. 1.4%) and 303 MPa (cov. 6.01%) vs 289 MPa (cov. 5.4%), respectively.

4.3. Effect of platelet length-to-thickness ratio

It was previously shown [31] that a greater platelet length-to-thickness (L_p/t_p) aspect ratio improves stress sharing in a composite system of aligned platelets and increases effective tensile strength due to shifting the dominant damage mode from platelet delamination to platelet tensile fracture. The subject of this section is to study how failure is produced in a composite system with $[0^{\circ}_{1/2}/45^{\circ}/90^{\circ}/-45^{\circ}/0^{\circ}_{1/2}]$ stacking of planar arrays of staggered platelets depending on the platelet length-to-thickness aspect ratio. The sampled morphology of a composite system is shown in Fig. 9(a). The non-periodic RVE (a computational window) has global dimensions of 12.75 mm (0.5020 in) by 12.75 mm (0.5020 in) along the x_1 and x_2-axes, respectively, and is the smallest volume that contains all the essential information about system meso-scale heterogeneities. The study investigates initiation and propagation of damage zones in the composite system under uniform uniaxial tension. The platelet length of $L_p = 12.7$ mm $= 0.5$ in is considered and $L_p/w_p = 4$. The platelet thickness, t_p, is a variable quantity. Therefore, the deterministic overlap distribution between platelets for various L_p/t_p ratios is preserved and the system morphology is fixed. The variation of effective composite response now only depends on the load transfer determined by the platelet geometrical aspect ratio. The outer 0°-layes were of half platelet thickness, so the total thickness of an

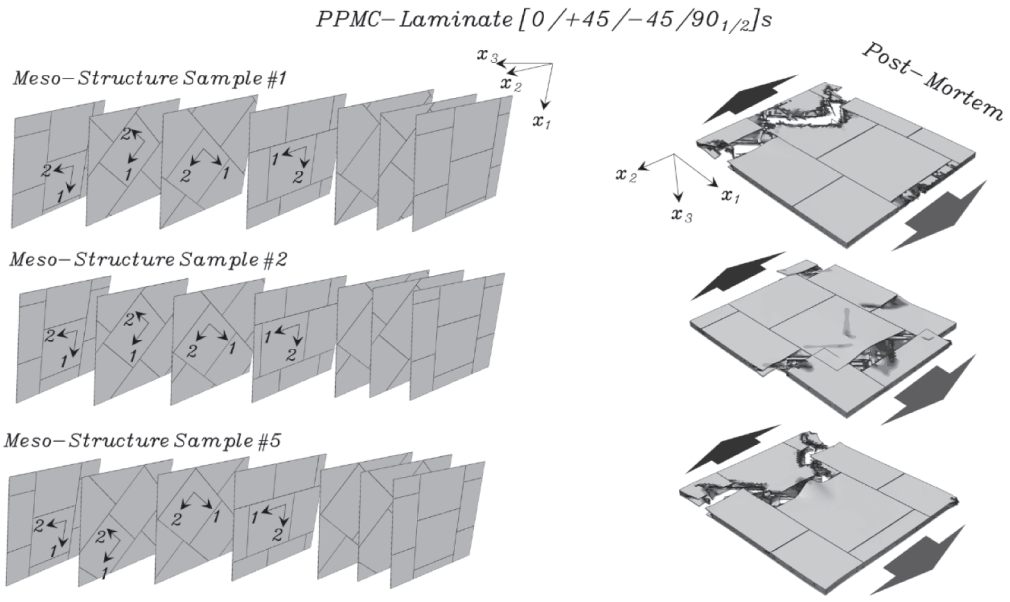

(a)

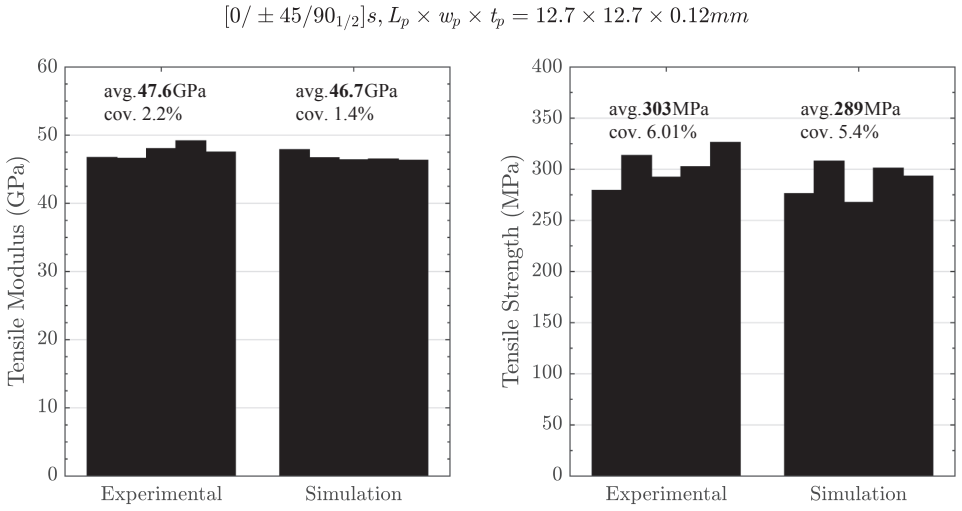

(b)

Fig. 8. Morphology caused variability of effective tensile properties of the $[0/\pm 45/90_{1/2}]_s$ PPMC-laminate, $L_p \times w_p \times t_p = 12.7 \times 12.7 \times 0.12$ mm: (a) Representative meso-structure samples showing the layer architecture and PPMC-laminate post-mortem; (b) Simulated distribution of tensile stiffness and strength.

RVE was $4t_p$. Periodic boundary conditions are applied to all RVE faces.

Fig. 9(b) shows the simulated effective response, $\bar{\sigma}_{11}(\bar{\epsilon}_{11})$, of a $[0^\circ_{1/2}/45^\circ/90^\circ/-45^\circ/0^\circ_{1/2}]$-composite system for a range of platelet thickness values, t_p, from 0.050 mm to 0.300 mm. The composite ultimate strength and stiffness plotted as a function of the L_p/t_p are also summarized in Fig. 9(b). The improved composite performance in tension is found for platelets of a greater L_p/t_p ratio. For small platelet L_p/t_p ratios, the inefficient stress transfer between platelets does not allow the strength of the platelet fibers contribute to the composite strength. The composite effective strength is reduced since the delaminations between platelets are substantial and zero-degree platelets do not experience fiber fracture since they do not support enough tensile stress. The failure modes of morphology samples corresponding to various platelet L_p/t_p ratios are shown in Fig. 10. Failure topology is defined by the complex interaction between platelet size and fixed PPMC meso-scale morphology and is presented with the pattern of the damage index, D. In Fig. 10, the undamaged and damaged elements are identified by the light grey ($D = 0$, no crack) and solid black ($D = 1$, local crack), respectively, with damage index defined as $D = \max(d_1, d_2, d)$. Failure topology in arrays with thinner platelets differed from that of the intermediate thickness platelets. For an increased L_p/t_p ratio, the improved stress sharing hinders delamination cracks propagation allowing platelet fibers to support more stress. When the fracture is less confined to the platelet-to-platelet interfaces and more extensive platelet fiber breakage is observed, it results in the enhanced composite effective tensile strength.

4.4. Effect of platelet length-to-width ratio

The objective of this section is to study the platelet width effect on tensile strength of a platelet array. A $[0^\circ/\pm 45^\circ/90^\circ/\mp 45^\circ/0^\circ]$ PPMC laminate is considered for a fixed platelet length and thickness of

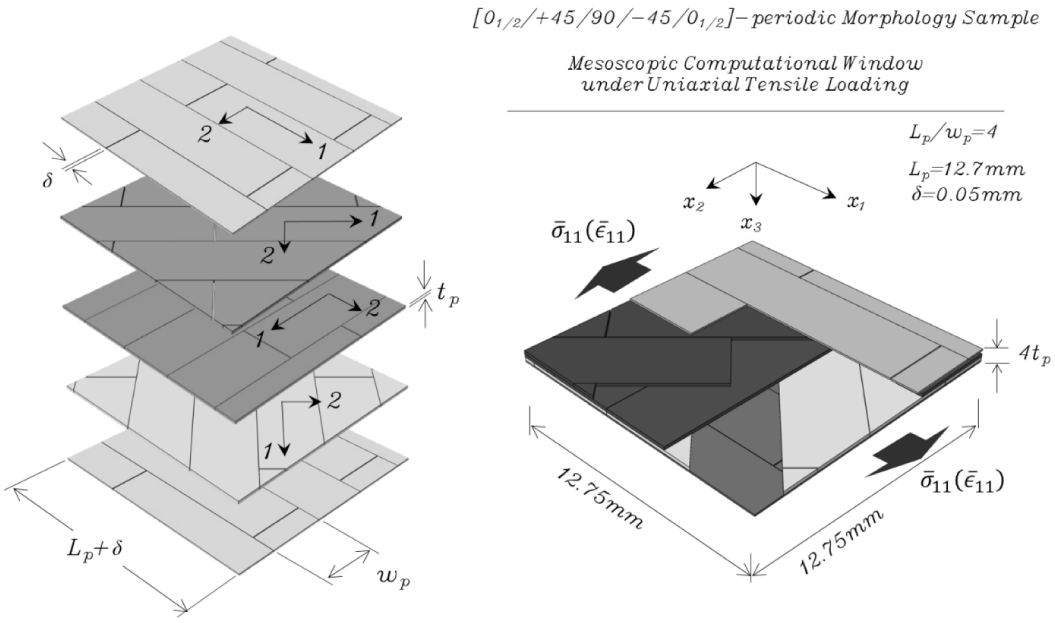

(a)

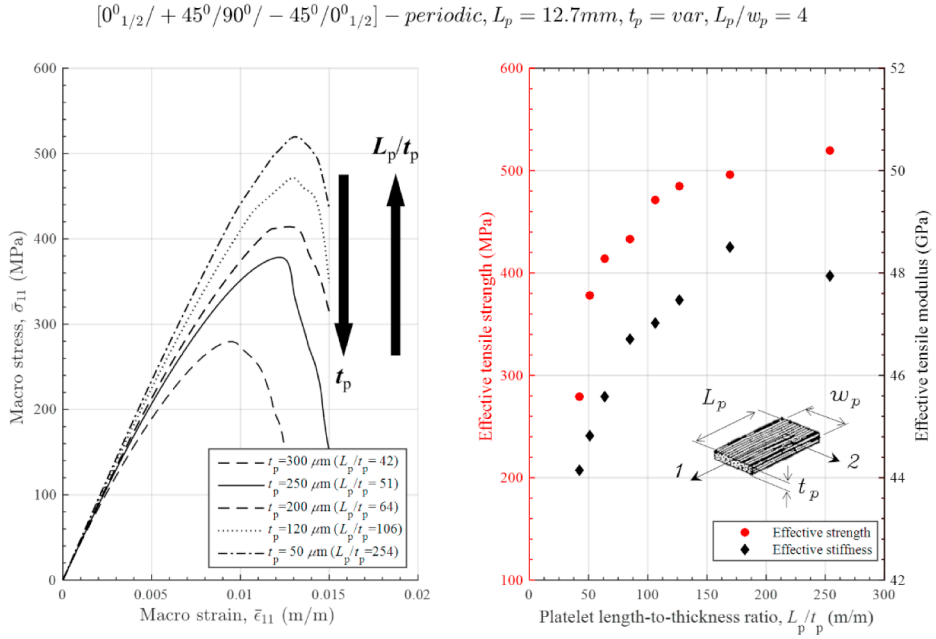

(b)

Fig. 9. (a) Composite system with $[0_{1/2}/45/90/-45/0_{1/2}]$ stacking of planar arrays of staggered platelets; (b) Effective composite stiffness and strength vs platelet L_p/t_p-ratio (platelet length L_p = 12.7 mm = 0.5 in; L_p/w_p = 4).

L_p = 12.7 mm and t_p = 0.12 mm. The non-periodic RVE (computational window) dimensions along the global x_1 and x_2 directions are 25.4 x 25.4 mm (1 x 1 in), while the RVE thickness is $7t_p$. Periodic boundary conditions are only applied on the x_1-faces with x_1 being the loading direction. Variation of platelet width (w_p) results in a modified PPMC meso-scale morphology since the distribution of platelets overlaps changes. Besides, a greater number of platelets in the composite system results from choosing a greater length-to-width aspect ratio if the platelet length is preserved. The platelets count variation influences the system degree of redundancy. Therefore, added redundancy, but preserved (unchanged) orientation state are the characteristics of the composite when a platelet width is reduced.

Fig. 11 (a) shows the effective stress-strain curves, $\bar{\sigma}_{11}(\bar{\epsilon}_{11})$, and the summary of composite tensile strength as a function of the platelet L_p/w_p-ratio. For the $[0^\circ/\pm 45^\circ/90^\circ/\mp 45^\circ/0^\circ]$ PPMC laminate, a platelet L_p/w_p-ratio increases from one to eight and translates into the substantially improved composite effective strength, while the effective modulus is much less affected. Non-monotonic improvement of strength with increased platelet L_p/w_p-ratio is caused by the local morphological effects of composite structure, i.e. the arrangement of overlaps between

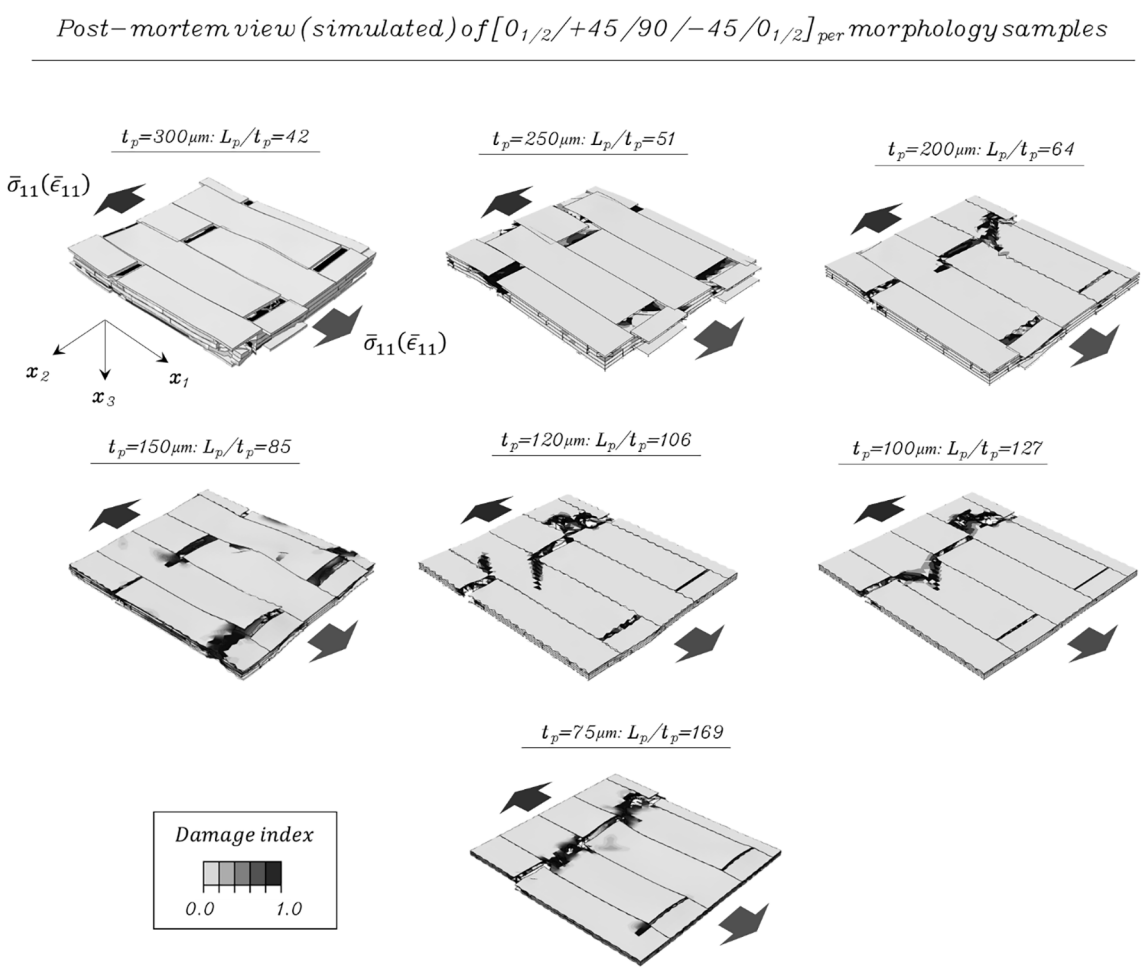

Fig. 10. Topology of a macro-cracks defined by the composite structure details (interaction between a platelet aspect ratio and fixed system morphology).

platelets. The composite strength increase for narrower platelets is a manifestation of the effect of added redundancy. There is an increased number of overlaps between a greater number of platelets, so the fracture path through the composite meso-structure becomes more tortuous, therefore more external work is needed to produce composite ultimate failure. On the other hand, increased number of overlapping areas implies that these areas are more uniformly and highly stressed. Therefore, by further reducing the platelet width, one would keep increasing the number of highly stressed (and potentially weak) overlaps between platelets, which should eventually override and suppress the benefit of having more redundancy. It is seen as the retardation of effective strength improvement for greater magnitudes of L_p/w_p ratio in Fig. 11(a).

Fig. 11(b) compares the failure paths in the composite systems of platelets for several different L_p/w_p ratios. It follows that the damage distribution is strongly affected by the meso-scale morphological characteristics of the composite system, since damage in the composite seeks out the locations where a local meso-scale stress concentration yields the most desirable failure sites.

5. Conclusions

In this work, the tensile properties of a prepreg platelet molded composite (PPMC) system with a deterministic orientation state achieved by engineering the meso-scale morphology of composite during the preforming stage were investigated. Specifically, the material form is a PPMC-laminate with multiple orientation of layers each of which contains aligned and staggered platelets. Experimental work allowed quantitative evaluation of the composite property improvements caused by the controlled morphology formation. Designed orientation state in a PPMC along with enhanced hierarchical arrangement of prepreg platelets results in controlled improvement of effective composite properties with reduced variability as compared to the stochastic PPMC. The benefit of designed orientation state was demonstrated by comparing the tensile properties of a PPMC-laminate to the tensile properties of a PPMC with a(n) stochastic/uncontrolled orientation state. Experimental results also showed that decreasing the platelet width might substantially improve effective strength of a PPMC-laminate by added structural redundancy.

Progressive failure analysis (PFA) of a PPMC-laminate was performed on samples with virtual morphology. Mechanical properties of individual platelets and their interfaces were taken as the properties of the platelet precursor material (UD CF tape) and used as input for the analysis to predict the macro response of the PPMC. The theoretical failure analysis allows for study of the composite effective strength as a function of composite structure descriptors and therefore an investigation of the structure-property relationship. PFA based on computational damage mechanics considered several interactive meso-scale failure modes in a PPMC-laminate such as in-platelet orthotropic damage modes and platelet-to-platelet delamination. The meso-scale damage modes in a PPMC-laminate are simultaneously competing during the fracture process.

The variable distribution of overlaps between platelets was shown to translate into the variability of effective tensile properties of a PPMC-laminate with a given orientation state. The simulated distribution of tensile properties of a PPMC-laminate caused by the variable meso-structure geometry is in a reasonable agreement with the experimental data. The thermal-residual stresses were found not to affect

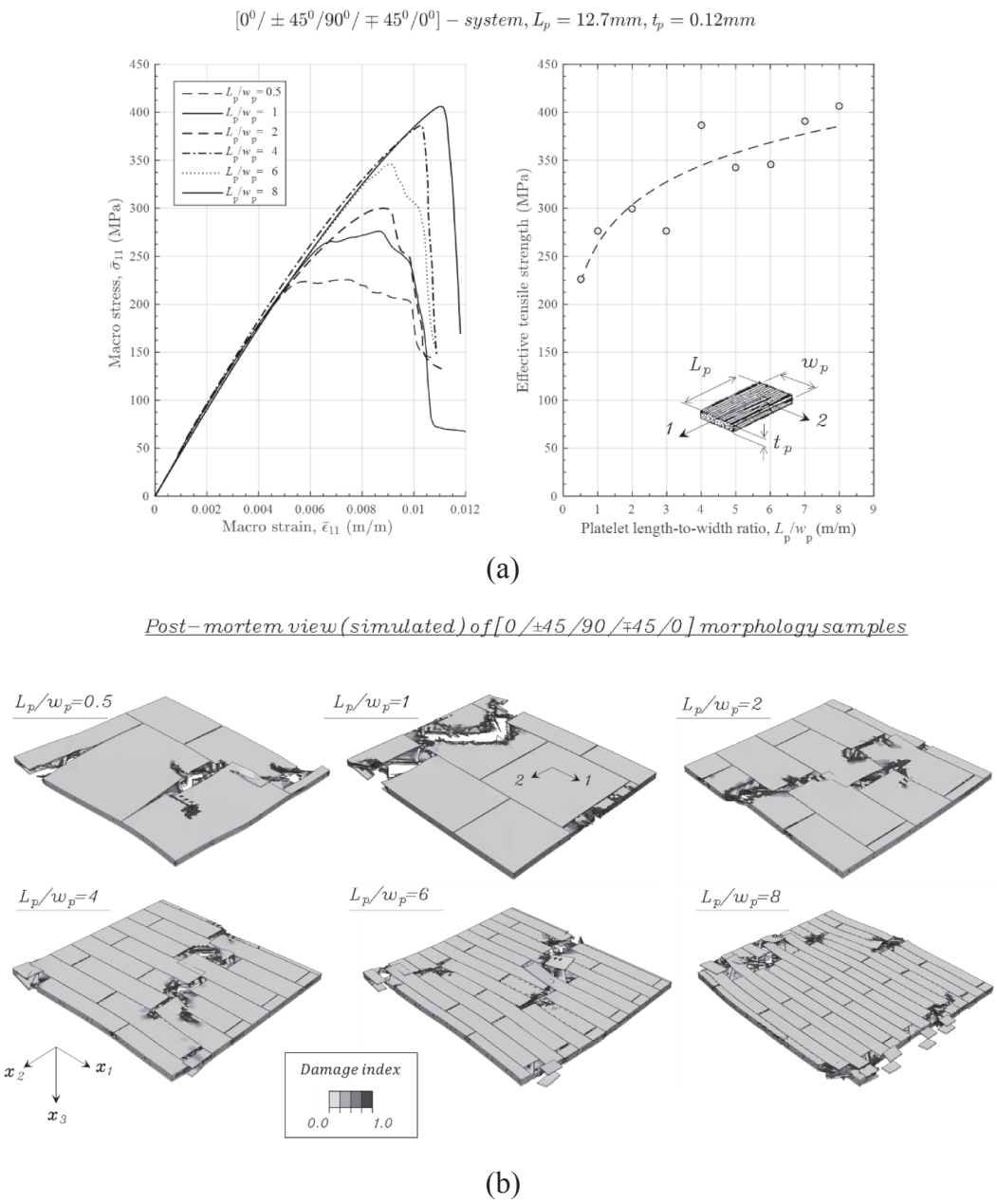

Fig. 11. (a) Effect of the platelet L_p/w_p ratio on effective tensile response of a [0°/ ± 45°/90°/∓45°/0°]-laminate of planar layers of aligned and staggered platelets; (b) Post-mortem view of layered morphology samples with various platelet length-to-width ratios (simulated results).

substantially the ultimate strength of a PPMC-laminate. The effects of the geometric platelet parameters on the macroscopic composite properties were investigated. It was shown that the platelet length-to-thickness ratio controls composite effective stiffness and strength improvement by controlling the meso-scale stress transfer efficiency. For a greater platelet length-to-thickness ratio, a platelet can support more axial stress while the delamination cracks development is retarder providing for the enhanced performance of the composite. The platelet width reduction introduces the increased internal redundancy and improved strength to the composite system. Although, the rate of strength improvement is retarded when platelet width is substantially reduced since it results in highly and uniformly stressed overlaps between platelets, which is not beneficial for stress transfer efficiency between platelets.

Appendix

The dynamic mechanical analysis (DMA) was used to determine the storage modulus of neat PEKK as a function of temperature. The analysis was performed using a Thermal Analyzer TA Instruments Q800 equipment operating in three-point bending horizontal measuring system. The experimental conditions used were dynamic force of 0.7 Nm, oscillating displacement of 10 μm, heating rate of 5 °C/min, and temperature range from 30 to 350 °C. DMA scans are shown in Fig. A1.

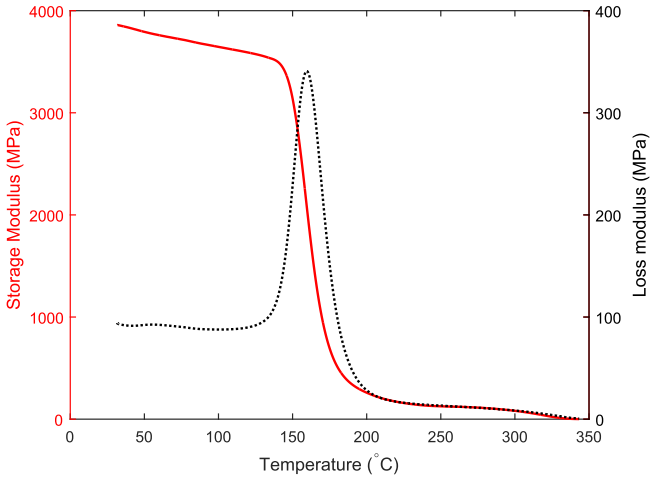

Fig. A1. DMA temperature scans of neat PEKK.

References

[1] Fudge JD. Chopped prepregs – compelling performance and cost effective material. SAMPE conference 41st ITSC, Wichita KS Oct 19–22nd, 2009. 2009.
[2] LeBlanc D, Landry B, Levy A, Hubert P, Roy S, Yousefpour A. Compression moulding of complex parts using randomly-oriented strands thermoplastic composites. In SAMPE. Seatle, WA; 2014.
[3] Taketa I, Okabe T, Matsutani H, Kitano A. Flowability of unidirectionally arrayed chopped strands in compression molding. Compos B Eng 2011;6(1764–1769):42.
[4] Feraboli P, Peitso E, Deleo F, Cleveland T. Characterization of prepreg-based discontinuous carbon fiber/epoxy systems. J Reinf Plast Compos 2009;28(10):1191–214.
[5] Courtney T. Fundamental structure-property relationships in engineering materials. ASM handbook, volume 20: materials selection and design. 1997. p. 336–56.
[6] Huang Z-M, Zhou Y-X. Strength of Multidirectional Laminates. Strength of fibrous composites. Berlin Heidelberg: Springer; 2011. p. 145–235.
[7] van Wijngaarden M, Jongbloed A, de Vries J. Thermoplastic compound compression molding. In SAMPE. Seatle WA, USA; 2010.
[8] Eguemann N, Giger L, Roux M, Dransfeld C, Thiebaud F. Compression moulding of complex parts for the aerospace with discontinuous novel and recycled thermoplastic composite materials. 19th international conference on composite materials. 2013.
[9] Yamashita S, Hashimoto K, Suganuma H, Takahashi J. Experimental characterization of the tensile failure mode of ultra-thin chopped carbon fiber tape-reinforced thermoplastics. J Reinf Plast Compos 2016;35(18):1342–52.
[10] Selezneva M, Lessard L. Characterization of mechanical properties of randomly oriented strand thermoplastic composites. J Compos Mater 2015.
[11] Nicoletto G, Riva E, Stocchi A. Mechanical characterization of advanced random discontinuous carbon/epoxy composites. Mater Today Proc 2016;3(4):1079–84.
[12] Jin BC, Li X, Jain A, González C, LLorca J, Nutt S. Optimization of microstructures and mechanical properties of composite oriented strand board from reused prepreg. Compos Struct 2017;174:389–98.
[13] Taketa I, Okabe T, Kitano A. A new compression-molding approach using unidirectionally arrayed chopped strands. Compos A 2008;39:1884–90.
[14] Taketa I, Sato N, Kitano A, Nishikawa M, Okabe T. Enhancement of strength and uniformity in unidirectionally arrayed chopped strands with angled slits. Compos A Appl Sci Manuf 2010;41(11):1639–46.
[15] Li Y, Pimenta S, Singgih J, Nothdurfter S, Schuffenhauer K. Experimental investigation of randomly-oriented tow-based discontinuous composites and their equivalent laminates. Compos A Appl Sci Manuf 2017;102:64–75.
[16] Li H, Wang W-X, Matsubara T. Multiscale analysis of damage progression in newly designed UACS laminates. Compos A Appl Sci Manuf 2014;57:108–17.
[17] Xue J, Wang W-X, Zhang J-Z, Wu S-J. Progressive failure analysis of the fiber metal laminates based on chopped carbon fiber strands. J Reinf Plast Compos 2015;34(5):364–76.
[18] Xue J, Wang W-X, Zhang J-Z, Wu S-J, Li H. Experimental and numerical study on the tensile behaviour of UACS/Al fibre metal laminate. Appl Compos Mater 2015;22(5):489–505.
[19] Feraboli P, Cleveland T, Stickler P, Halpin J. Stochastic laminate analogy for simulating the variability in modulus of discontinuous composite materials. Compos A Appl Sci Manuf 2010;41(4):557–70.
[20] Selezneva M, Roy S, Lessard L, Yousefpour A. Analytical model for prediction of strength and fracture paths characteristic to randomly oriented strand (ROS) composites. Compos B Eng 2016;96:103–11.
[21] Sato Y, Takahashi J, Matsuo T, Ohsawa I, Kiriyama K, Nagoh S. Elastic modulus estimation of chopped carbon fiber tape reinforced thermoplastics using the Monte Carlo simulation. ICCM-19, 19th international conference on composite materials. 2013.
[22] Carlsson LA, Adams DF, Pipes RB. Basic experimental characterization of polymer matrix composite materials. Polym Rev 2013;53(2):277–302.
[23] Dassault Systèmes, ABAQUS. ABAQUS documentation. Providence, RI; 2016.
[24] Such M, Ward C, Potter K. Aligned discontinuous fibre composites: a short history. J Multifunct Compos 2014;3:155–68.
[25] Denos BR, Sommer DE, Favaloro AJ, Pipes RB, Avery WB. Fiber orientation measurement from mesoscale CT scans of prepreg platelet molded composites. Compos A Appl Sci Manuf 2018;114:241–9.
[26] Hartmann M, Schwieger W. Hierarchically-structured porous materials: from basic understanding to applications. Chem Soc Rev 2016;45(12):3311–2.
[27] Böhm HJ. A short introduction to basic aspects of continuum micromechanics. ILSB Reports/ILSB-Arbeitsbericht 206. Vienna; 2012.
[28] Ostoja-Starzewski M. The use, misuse, and abuse of stochastic random media. Proceedings of European conference on computational mechanics. 2001.
[29] Suquet P. Elements of homogenization theory for inelastic solid mechanics. Homogenization techniques for composite media. Berlin: Springer-Verlag; 1987. p. 194–275.
[30] Cox H. The elasticity and strength of paper and other fibrous materials. Br J Appl Phys 1952;3:72–9.
[31] Kravchenko S, Sommer D, Pipes B. Uniaxial strength of a composite array of overlaid and aligned prepreg platelets. Compos A Appl Sci Manuf 2018;109:31–47.
[32] Lapczyk I, Hurtado J. Progressive damage modeling in fiber-reinforced materials. Composites A 2007;38:2333–41.
[33] Hashin Z. Failure criteria for unidirectional fiber composites. J Appl Mech 1980;47:329–34.
[34] Bazant Z, Oh B. Crack band theory for fracture of concrete. Mater Struct 1983;16:155–77.
[35] PEKK thermoplastic polymer. Technical Data Sheet. Cytec; 2012.
[36] Brewer J, Lagace P. Quadratic stress criterion for initiation of delamination. J Compos Mater 1988;22(12):1141–55.
[37] Whitcomb J. Analysis of instability-related growth of through-thickness delamination. NASA TM-86301.
[38] Gong XJ, Hurez A, Verchery G. On the determination of delamination toughness by using multidirectional DCB specimens. Polym Test 2010;29(6):658–66.
[39] Forghani A, Shahbazi M, Zobeiry N, Poursartip A, Vaziri R. An overview of continuum damage models used to simulate intralaminar failure mechanisms in advanced composite materials. Numerical modeling of failure in advanced composite materials. Elsevier; 2015.
[40] Davilla CG, Camanho P, Turon A. Effective simulation of delamination in aeronautical structures using shells and cohesive elements. J Aircrafts 2008;45(2).
[41] Henninger HB, Reese SP, Anderson AE, Weiss JA. Validation of computational models in biomechanics. Proc Inst Mech Eng Part H J Eng Med 2010;224(7):801–12.
[42] Council NR. Model validation and prediction. Assessing the reliability of complex models: mathematical and statistical foundations of verification, validation, and uncertainty quantification. National Academies Press; 2012. p. 52–85.
[43] Carley KM. Validating computational models; 1996. [Online]. Available: http://www.casos.cs.cmu.edu/publications/papers.php.
[44] Tzeng JT. Predictions and experimental verification of residual stresses in thermoplastic composite cylinders. J Thermoplast Compos Mater 1995;8(2):163–79.
[45] Jeronimidis G, Parkyn AT. Residual stresses in carbon fibre-thermoplastic matrix laminates. J Compos Mater 1988;22(5):401–15.